Magnetic and thermodynamic properties of the spin-dimer system La_2RuO_5 induced by Mn substitution

S. Riegg,[1,*] A. Wintermeier,[1] H.-A. Krug von Nidda,[1] S. Widmann,[1] A. Günther,[1] A. Reller,[2] S. G. Ebbinghaus,[3] and A. Loidl[1]

[1]*Experimental Physics V, Center for Electronic Correlations and Magnetism, University of Augsburg, D-86159 Augsburg, Germany*

[2]*Resource Strategy, University of Augsburg, D-86159 Augsburg, Germany*

[3]*Solid State Chemistry, Martin-Luther-University Halle-Wittenberg, D-06099 Halle, Germany*

(Received 4 February 2014; revised manuscript received 13 June 2014; published 14 July 2014)

Magnetic properties as well as the specific heat of the spin-dimer system $La_2Ru_{1-y}Mn_yO_5$ were investigated for manganese concentrations $0 \leqslant y \leqslant 0.25$. The magnetic (dc) susceptibility of the unsubstituted ($y = 0$) system shows a steplike decrease close to 160 K reflecting a magnetostructural transition into a dimerized ground state. With increasing manganese concentration this behavior (typical for singlet formation) becomes continuously suppressed and the susceptibility bears the signatures of the emergence of new magnetic ground states. The high-temperature Curie-Weiss susceptibility can be described by Ru^{4+} ($S = 1$) and Mn^{4+} ($S = \frac{3}{2}$) spin moments, with a dramatic decrease of the Curie-Weiss temperatures by almost 30% close to $y = 0.1$, indicating significant changes in the average mean magnetic exchange. Field-cooled and zero-field-cooled experiments as well as ac-susceptibility measurements provide clear evidence for the formation of a spin-glass state, well below the characteristic dimerization temperature. The relaxation dynamics can be described by a Vogel-Fulcher-Tammann behavior and indicates high fragility when characterized in terms of glassy dynamics of canonical supercooled liquids. Additional electron-spin resonance experiments indicate different spin-glass regimes and a rather dynamic nature of the dimerized phase. In the Mn-substituted compounds, a linear contribution to the heat capacity at low temperatures can be ascribed to the spin-glass formation. With increasing manganese concentration, the anomaly in the specific heat caused by the spin-singlet formation is shifted to lower temperatures and becomes continuously suppressed and smeared out. On the basis of these results, we propose a (y,T)-phase diagram indicating the competition of the spin-glass and the dimerized states. We stress the similarities with doped $CuGeO_3$, the canonical inorganic spin-Peierls system.

DOI: 10.1103/PhysRevB.90.024407 PACS number(s): 75.30.Cr, 75.30.Kz, 75.50.Lk, 76.30.−v

I. INTRODUCTION

The substitution of Ru by Mn in perovskite-related compounds leads to a large variety of structural modifications and concomitant diverse physical properties. Especially, a variety of magnetic phases is observed due to the diversity of possible exchange interactions of localized Mn and localized or itinerant Ru moments in these compounds. Furthermore, the various possible oxidation states for Ru and Mn even increase the variability of interactions. For example, the perovskite $SrRu_{1-x}Mn_xO_3$ provides a complex magnetic phase diagram [1]. It involves a transition from a paramagnetic high-temperature phase to a ferromagnetically ordered low-temperature state at low substitution levels x, with itinerant Ru 4*d* electrons and metallic conductivity. In contrast, on the Mn-rich side, an antiferromagnetically ordered and insulating phase with localized moments is observed with a Néel temperature of approximately 200 K. For intermediate concentrations x, spin-glass and cluster-glass phases are observed [1]. Cao *et al.* reported a possible quantum-critical point (QCP) for $x \approx 0.39$, at which the ferromagnetic ordering turns into an antiferromagnetic arrangement at zero temperature [2]. In addition, magnetoresistance at low temperatures was reported for the samples with intermediate substitution levels [1]. Partial replacement of Sr by Ca shifts the QCP to $x = 0.2$ and a substitution by trivalent La decreases the temperature of the magnetic phase transitions [3,4].

Recently, substitution series of Ru by Mn were also reported for the perovskite-related compounds $CaCu_3Ru_{4-x}Mn_xO_{12}$ ($0 \leqslant x \leqslant 3$), which belong to the $AA'_3B_4O_{12}$ family of cation-ordered perovskites [5,6]. The ruthenate $CaCu_3Ru_4O_{12}$ is a Pauli paramagnet with itinerant charge carriers showing heavy-fermion behavior [7]. For this compound, non-Fermi-liquid [8] and intermediate-valence behavior [9] were reported. Strong correlation effects were also observed for the rare-earth-substituted $LnCu_3Ru_4O_{12}$ (Ln = La, Pr, Nd) [10,11]. On the other hand, the manganite $CaCu_3Mn_4O_{12}$ is a half-metallic ferromagnet and provides colossal magnetoresistance properties up to 280 K [12]. In $CaCu_3Ru_{4-x}Mn_xO_{12}$ significant changes of the physical properties are observed with increasing manganese concentration x [6].

Layered manganites of the perovskite-related Ruddlesden-Popper family have also been substituted with Ru. The manganites $(La,Sr)_{n+1}Mn_nO_{3n+1}$ provide different giant magnetoresistance properties depending on n and, in turn, on the dimensionality of the MnO_6-octahedra network [13,14]. For $n = 1$ ($Sr_2Mn_xRu_{1-x}O_4$) and $n = 2$ ($Sr_3Mn_xRu_{2-x}O_7$), partial substitution of Mn by Ru was reported and phase transitions from a paramagnetic phase albeit with ferromagnetic Curie-Weiss temperatures to a cluster-glass and spin-glass phase were observed [15–17]. Lanthanum-containing compounds $La_{1.2}Sr_{1.8}Mn_{2-x}Ru_xO_7$ ($n = 2$) with Ru substitution levels up to $x = 0.5$ show a rather complex antiferromagnetic order [18,19]. Complex magnetic ordering in these compounds is basically caused by the different valence states of Ru^{4+}/Ru^{5+} and Mn^{3+}/Mn^{4+} and by the fact that the electrons behave somewhat in-between localized and itinerant. The various

*stefan.riegg@physik.uni-augsburg.de

d-electron configurations lead to a large number of magnetic interactions between the ions and to the magnetoresistance effects. The ferromagnetic double-exchange mechanism competes with the antiferromagnetic superexchange, leading to different magnetic ground states depending also on structural changes.

The structure of $La_2Ru_{1-y}Mn_yO_5$ can be described as alternating layering of perovskite like La(Ru/Mn)O_4 and LaO layers similar to the $n = 1$ Ruddlesden-Popper system. Pure La_2RuO_5 shows a magnetostructural phase transition at 161 K [20,21]. Upon cooling, the crystal structure changes from monoclinic [$P2_1/c$, No. 14, high-temperature (ht) phase] to triclinic [$P\bar{1}$, No. 2, low-temperature (lt) phase], and due to the emerging structural changes the Ru-spin moments ($S = 1$) of the paramagnetic ht phase form a spin-singlet ground state of dimerized Ru spins being arranged as rungs of a ladderlike magnetic structure. Furthermore, caused by this transition, the electronic conductivity of the semiconducting La_2RuO_5 decreases with an increase of the band gap from 0.15 eV in the high-temperature phase to 0.21 eV in the low-temperature modification [20,22–26].

Inorganic spin-dimer systems showing a spin-Peierls transition are very rare; only $CuGeO_3$ and TiOCl were reported as typical representatives [27–29]. In these systems, $S = \frac{1}{2}$ spin moments are involved. Especially for TiOCl the spin-Peierls character of the dimerization is at least controversially discussed and doping leads to a behavior typical for a Luttinger liquid [29–32]. Even rarer are low-dimensional $S = 1$ systems showing a spin gap. Examples are La_2RuO_5 and $PbNi_2V_2O_8$. While $PbNi_2V_2O_8$ can be described as a one-dimensional (1D) Haldane system [33], La_2RuO_5 shows a two-dimensional (2D) spin-Peierls-like transition. Due to the perturbance of the magnetic system by doping, in $CuGeO_3$ and $PbNi_2V_2O_8$, a long-range-ordered antiferromagnetic phase is established at low temperatures [33–35]. Similar perturbance or impurity-induced effects are also expected for Mn-substituted La_2RuO_5 and will be discussed in the following.

Synthesis and magnetic as well as heat-capacity characterizations of $La_2Ru_{1-y}Mn_yO_5$ have been further motivated by the fact that in this solid solution spin-singlet formation competes with magnetic exchange interactions, presumably yielding a complex phase diagram and exotic ground states.

The crystal structure of $La_2Ru_{1-y}Mn_yO_5$ was investigated in detail depending on temperature and substituton level y (Ref. [36]). In addition, the valence states of Ru and Mn were determined by x-ray absorption spectroscopy documenting that both ions are purely tetravalent, at 300 K as well as at 110 K.

In this work, the dc- and ac-magnetic susceptibilities of $La_2Ru_{1-y}Mn_yO_5$ are investigated as a function of temperature. Furthermore, magnetization curves of the samples were recorded in a field range of ± 5 T for various temperatures and electron-spin resonance (ESR) measurements were performed. In addition, the specific heat was evaluated for selected samples. From the experimental results, the relationship between changes in crystal structure with magnetic and thermodynamic properties is discussed. Combining all experimental results, a detailed (y,T)-phase diagram of $La_2Ru_{1-y}Mn_yO_5$ is proposed.

II. EXPERIMENTAL METHODS

Magnetic properties were measured in the temperature range $2 \leqslant T \leqslant 400$ K using a SQUID magnetometer (Quantum Design MPMS-XL). The dc susceptibility was measured in an external field of $\mu_0 H = 0.1$ T in field-cooled (fc) mode. Additional measurements in both fc and zero-field-cooled (zfc) mode were carried out in $\mu_0 H = 10$ mT. For the isothermal magnetization measurements, $\mu_0 H$ was varied between ± 5 T. ac susceptibility was measured for frequencies between 1 Hz and 1 kHz applying an ac field of 0.2 mT. The powder samples were enclosed in gel capsules, whose small contributions to the measured susceptibility were taken into account by including a temperature-independent susceptibility χ_0.

The ESR spectra were measured at constant microwave frequency of $\nu \approx 9.4$ GHz (X band) as function of a static external magnetic field using a Bruker ELEXSYS E500 CW spectrometer. This ESR spectrometer is equipped with a continuous He-gas flow cryostat (Oxford Instruments) working in the temperature range from liquid helium to room temperature. Due to lock-in technique with field modulation, the field derivative of the absorption spectra was recorded.

The specific heat C_p was determined using a physical property measurement system (Quantum Design PPMS) in the temperature range $1.8 \leqslant T \leqslant 300$ K in steps of 1 K. In the vicinity of the phase transition peak (± 15 K) and below 30 K, a step width of 0.2 K was chosen. Approximately 10 mg of sample powder and 2 mg of polyvinyl-alcohol (PVA) were mixed, ground in an agate mortar and pressed into pellets of 3 mm diameter. The PVA contribution to C_p was subtracted taking into account the exact weight fraction. The fit of the lattice contribution to C_p was carried out using the program MATHEMATICA 7 and an Einstein-Debye phonon model.

III. EXPERIMENTAL RESULTS AND DISCUSSION

A. Magnetic properties

In the low-temperature (lt) phase of undoped La_2RuO_5, the spin dimerization results from structural changes close to 160 K with the formation of alternating longer and shorter Ru-Ru distances and a concomitant singlet formation of two neighboring Ru^{4+} spin moments along the crystallographic b direction [26]. A partial replacement of Ru^{4+} with $S = 1$ by Mn^{4+} with $S = \frac{3}{2}$ is expected to have a strong influence on the singlet formation and to lead to a complex magnetic ground state. As spin dimerization and structural phase transition are intimately coupled, the effect of Mn substitution on the crystal structure in general and especially on the low-temperature structural transition was studied in detail using (synchrotron) x-ray and neutron diffraction [36]. For manganese substitution levels up to $y = 0.2$, a complete transition to the triclinic lt phase was observed, while for $y = 0.25$ only about 45% of the high-temperature phase transforms into the low-temperature modification, in which this characteristic dimerization occurs (Ref. [36]).

1. dc susceptibility and magnetization

Figures 1(a) and 1(b) show the magnetic dc susceptibility of $La_2Ru_{1-y}Mn_yO_5$ for manganese concentrations $0 \leqslant y \leqslant 0.25$ and temperatures between 1.5 and 400 K. The magnetic

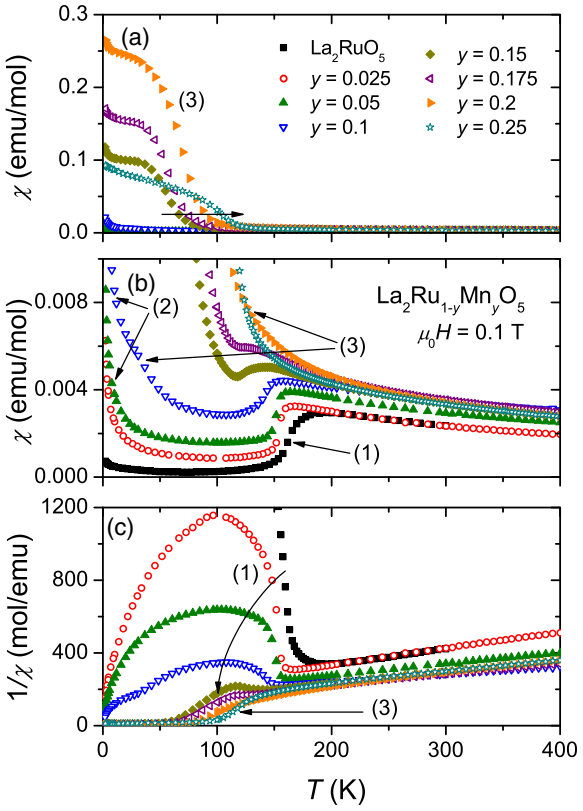

FIG. 1. (Color online) (a) Temperature-dependent magnetic dc susceptibility of $La_2Ru_{1-y}Mn_yO_5$. (b) Details of the susceptibility on enlarged scale. (c) Corresponding temperature-dependent inverse susceptibilities. The numbers correspond to the different magnetic phases according to (1) Ru-Ru spin dimerization, (2) paramagnetic Curie tail of nondimerized Ru and Mn spin moments, and (3) Ru-Mn spin interactions. For details, see text.

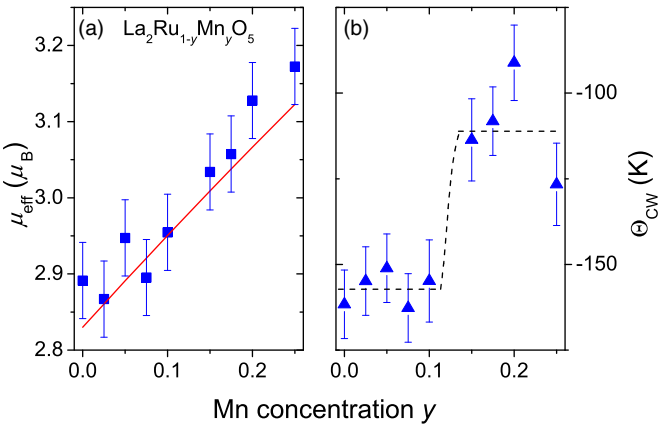

FIG. 2. (Color online) Effective paramagnetic moments μ_{eff} (a) and Curie-Weiss temperatures Θ_{CW} (b) for $La_2Ru_{1-y}Mn_yO_5$ determined from fits to the high-temperature range of $1/\chi$ (190–400 K). The solid line in (a) indicates the theoretically expected paramagnetic moments. The dashed line in (b) is drawn to guide the eye. For details, see text.

susceptibility $\chi = M/H$ has been determined in an external field $\mu_0 H = 0.1$ T for all concentrations. Figure 1(c) shows the inverse susceptibility. Figure 1(a) clearly documents that for some samples a small but significant spontaneous magnetization evolves below approximately 120 K. This effect only appears for Mn concentrations $y \geqslant 0.15$ and the onset temperature increases with increasing y (as indicated by the horizontal arrow). The ordered moment reaches a maximum close to $y = 0.2$ and decreases again on further increasing manganese substitution. This behavior can be attributed to noncompensated (ferrimagnetic) Ru-Mn spin pairs with a residual spin of $S = \frac{1}{2}$, but also could be a sign of the formation of a spin-glass state.

Zooming into the low-temperature susceptibility, Fig. 1(b) documents that dimerization with spin-singlet formation is visible as a steplike decrease of the susceptibility between 100 and 160 K and can clearly be detected up to Mn concentrations $y = 0.175$ [the dimerization is indicated as process (1) in Fig. 1]. The dimerization transition becomes smeared out, the susceptibility step becomes smaller, and the transition temperature decreases upon further increasing substitution with an onset close to 120 K for $y = 0.175$. At the lowest temperatures, a Curie tail develops with increasing Mn concentration [feature (2) in Fig. 1(b)]. This Curie tail most likely results from isolated ruthenium or manganese spins of unpaired neighbors. The Curie component is very weak in the pure compound, increases drastically on substitution, and for $y \geqslant 0.1$ becomes dominated by the ferromagneticlike component [feature (3) in Fig. 1].

The inverse susceptibility [Fig. 1(c)] documents a Curie-Weiss behavior of the susceptibility at temperatures above 200 K and reveals a prominent increase at the onset of spin dimerization. The linear behavior of $1/\chi$ above T_d was fit by a Curie-Weiss law $\chi = C/(T - \Theta_{\text{CW}})$ including a small temperature-independent susceptibility χ_0 taking into account diamagnetic or van Vleck paramagnetic contributions. For all concentrations, χ_0 was found to be negligibly small ($<10^{-4}$ emu/mol) and is therefore not further discussed. From the Curie constant C, we calculated the paramagnetic moments for the different concentrations assuming spin-only moments with $g = 2$. The results are shown in Fig. 2(a). The paramagnetic moments increase almost linearly as a function of manganese concentration. With a valence of +4 for both ruthenium and manganese ions, as earlier determined by x-ray absorption near edge structure (XANES) measurements [36], paramagnetic moments of 2.83 μ_{B} for ruthenium ($S = 1$) and 3.87 μ_{B} for manganese ions ($S = \frac{3}{2}$) are calculated. The theoretical expectation is shown as a solid line in Fig. 2(a) and is in excellent agreement with the experimental results. It has to be mentioned, though, that also the possible combination of Mn^{3+} ($3d^4$: $S = 1$) and Ru^{5+} ($4d^3$: $S = \frac{3}{2}$) observed for other Ru/Mn compounds would lead to the same values for μ_{eff}. However, XANES measurements clearly prove the +4 oxidation states for both ions.

Figure 2(b) shows the Curie-Weiss temperatures as determined from the fits. For $0 \leqslant y \leqslant 0.1$, Θ_{CW} is close to -155 K but shows a steplike increase to approximately -110 K for higher manganese concentrations. This abrupt change of the Curie-Weiss temperature by roughly 30% is not easy to explain. It can certainly not be due to structural changes as these vary smoothly upon increasing concentration. One might assume that increasing manganese concentration

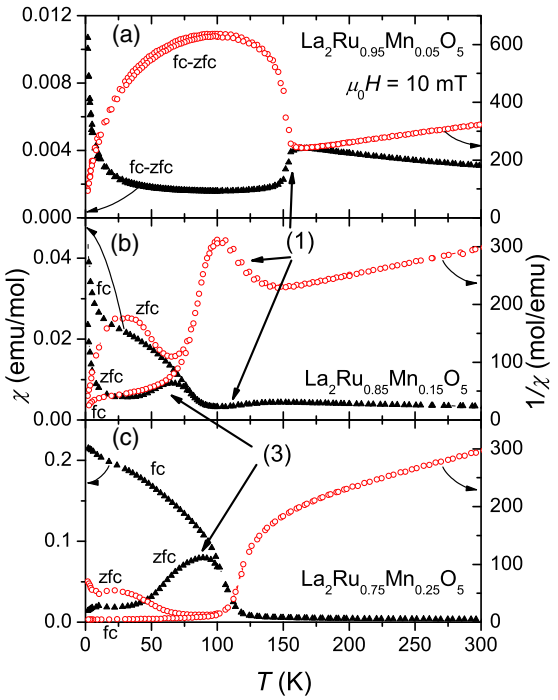

FIG. 3. (Color online) Temperature-dependent magnetic susceptibility (black triangles, left scale) and corresponding inverse susceptibility (open red circles, right scale) measured in fc and zfc modes at $\mu_0 H = 10$ mT for (a) $La_2Ru_{0.95}Mn_{0.05}O_5$, (b) $La_2Ru_{0.85}Mn_{0.15}O_5$, and (c) $La_2Ru_{0.75}Mn_{0.25}O_5$.

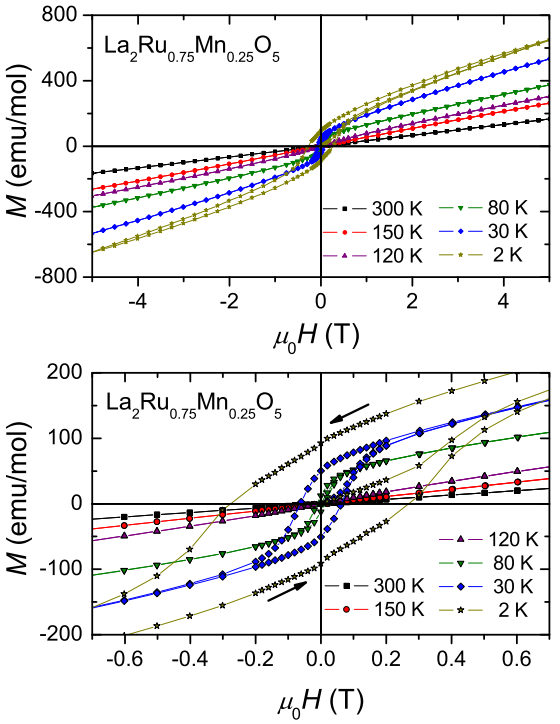

FIG. 4. (Color online) Magnetic hysteresis curves of $La_2Ru_{0.75}Mn_{0.25}O_5$ at 300, 150, 120, 80, 30, and 2 K. In the top frame the complete measurement range and in the bottom frame the detailed part close to the origin is shown. Arrows indicate the direction of increasing or decreasing external field $\mu_0 H$.

with a larger spin value increases the absolute value of the interaction, but the opposite effect is observed because the substitution changes the local environment of Ru. Obviously, the antiferromagnetic Ru-Ru interactions are stronger than the Ru-Mn interactions, probably because of the more extended 4*d* orbitals of ruthenium compared to the 3*d* orbitals of manganese. The steplike increase of the Curie-Weiss temperature very likely results from a percolation-type phenomenon: At a manganese concentration of approximately $y = 0.1$, every ruthenium ion has on the average one manganese ion at a neighboring site with a concomitant strong decrease in antiferromagnetic exchange.

To gain further insight into the lt-ordered state of the manganese-doped samples, we performed additional field-cooled (fc) and zero-field-cooled (zfc) experiments. The results are depicted in Figs. 3(a) ($y = 0.05$), 3(b) ($y = 0.15$), and 3(c) ($y = 0.25$) where we show fc and zfc susceptibilities as measured at $\mu_0 H = 10$ mT (black triangles, left scales) and the inverse susceptibilities (open red circles, right scales). For manganese contents $y < 0.1$ fc and zfc measurements are identical without significant splitting exceeding experimental uncertainties. As a prototypical example, we show the results for $y = 0.05$ [Fig. 3(a)]. The step in the susceptibility is well developed, as is a Curie tail of isolated noninteracting spins. In contrast, for $y = 0.1$, a splitting of fc and zfc shows up just below the dimerization transition (not shown). The results for $y = 0.15$ are depicted in Fig. 3(b). A smeared-out cusp in the susceptibility due to the spin-singlet formation is visible, but is much better documented in the inverse susceptibility. Below 100 K, the increase in χ signals the onset of weak ferromagnetism and subsequently fc and zfc susceptibilities split close to 75 K. In the fc as well as in the zfc measurement, a Curie tail can clearly be identified at low temperatures. Fc and zfc splitting possibly indicate domain dynamics of a weak ferromagnet, but might also indicate the onset of spin-glass freezing at a characteristic freezing temperature T_f. In Fig. 3(c), we show the results for $y = 0.25$. For this manganese concentration, which corresponds to the maximum substitution level, the dimerization transition can not be detected within experimental uncertainties and, thus, seems to be fully suppressed. This is clearly documented by the temperature dependence of the inverse susceptibility. The onset of spontaneous magnetization with a weak ferromagnetic moment at 120 K is followed by a fc-zfc splitting at 100 K.

Finally, we measured the magnetization as function of the external magnetic field. As an example, Fig. 4 shows the magnetization for $y = 0.25$ in the full accessible field range ($\mu_0 H \leqslant 5$ T) for a series of temperatures between 2 and 300 K [Fig. 4(a)] and a detailed view of the hysteresis on strongly enlarged scales [Fig. 4(b)]. Overall, this compound reveals predominantly paramagnetic behavior without saturation up to 5 T. However, clear hysteresis effects appear below 100 K, as documented by field sweeps at 2, 30, and 80 K. A ferromagnetic hysteresis develops with a remanence of 100 emu/mol and a coercive field of approximately 300 mT at 2 K. For the other compounds showing the splitting of fc and zfc susceptibility ($y \geqslant 0.1$) similar magnetization data were found, however, with significantly lower values for remanence and coercive field.

2. ac susceptibility

To identify possible spin-glass freezing, all samples exhibiting fc-zfc splitting ($0.1 \leqslant y \leqslant 0.25$) were investigated by ac measurements in zero external fields and at excitation frequencies between 1 Hz and 1 kHz. For selected concentrations, the real part of the ac susceptibilities is shown in Fig. 5 for five frequencies and temperatures below 120 K. A well-developed cusp with small but characteristic frequency dependence appears for all samples investigated. Usually, this cusplike feature in the real part of the ac susceptibility is taken as signature of spin-glass freezing. We are aware that in general models of glassy freezing the loss maximum would correspond to an average mean relaxation time. Here, however, we follow the standard spin-glass literature [37,38]. For $y = 0.1$, a single cusplike maximum in the ac susceptibility shows up at approximately 30 K followed by a frequency-independent increase towards low temperatures, signaling the contribution of free and noninteracting spins even in the spin-glass regime. For $y = 0.15$, the dominant frequency-dependent maximum is shifted to 75 K, but a second cusp appears at 40 K. With increasing manganese content, a clear double-peak structure arises, with both peaks shifted to higher temperatures. At $y = 0.25$, the peaks are located close to 80 and 100 K. In spin glasses, two-peak structures often are interpreted as the onset of spin-glass freezing at elevated temperatures followed by a blocking transition where the short-range-ordered clusters finally freeze out. In the case of $La_2Ru_{1-y}Mn_yO_5$ it is also possible that two subsystems of manganese spins with $S = \frac{3}{2}$ and ruthenium spins with $S = 1$ undergo subsequent glass transitions. We also have to recall that the spin-glass transitions for $y \leqslant 0.2$ appear in a dimerized matrix with a statistical distribution of spin singlets. Glassiness in spin systems results from disorder and frustration. In manganese-doped La_2RuO_5, frustration results from the competition of antiferromagnetic exchange with singlet formation, which strongly is coupled to the lattice. Disorder is due to a statistical distribution of Mn ions but also due to formed singlets. It is important to note that the spin-glass transition always appears just below the singlet formation. For $y = 0.25$, one might speculate that the two peaks result from the two different structural phases, which form close to 120 K and are the reminder of dimerization. However, the ac susceptibilities for $y = 0.2$ (not phase separated) and $y = 0.25$ (phase separated below 120 K) are very similar and we therefore do not think that the different structural phases show different glass transitions.

To gain further information of the spin-glass formation in $La_2Ru_{1-y}Mn_yO_5$, we analyzed the peak positions in the ac-susceptibility data in more detail. Unfortunately, the data for $y = 0.1$ are rather noisy due to a low susceptibility and the peak positions for $y = 0.2$ and 0.25 are difficult to analyze due to the appearance of double-peak structures. Hence, we focus on the results for $y = 0.15$.

The frequency dependence of the freezing temperature, as indicated by the temperature shift of the cusp maxima as a function of measuring frequency, can be used to gain insight into possible freezing mechanisms. For spin glasses, it was proposed to use $\Delta T_f/[T_f \cdot \Delta(\lg\omega)]$ as a quantitative measure [37]. If this equation can be applied down to zero frequency, the static freezing temperature is zero. By analyzing the real part of the ac susceptibility for $y = 0.15$, we derived a value of 0.0097, which is in the range of values observed in metallic spin glasses, such as, e.g., Cu:Mn compounds. In insulating spin glasses, such as (Eu/Sr)S, on the other hand, a distinctly stronger frequency dependence of T_f is observed. For these spin-glass systems, a Vogel-Fulcher-Tammann behavior was proposed to explain the observed

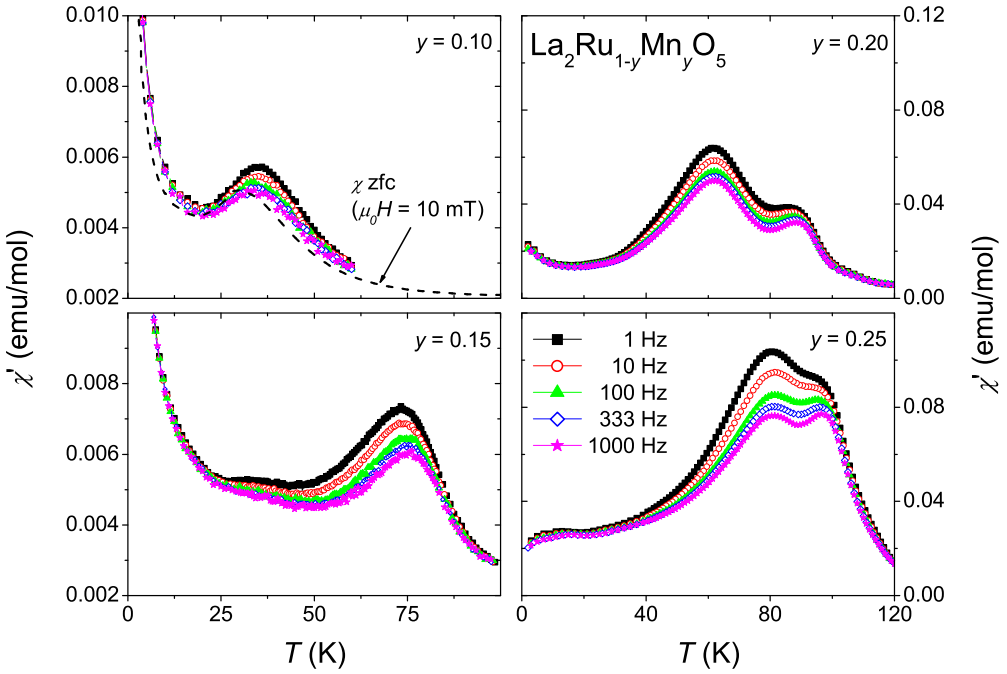

FIG. 5. (Color online) Temperature-dependent real parts (χ') of the ac susceptibilities of selected $La_2Ru_{1-y}Mn_yO_5$ samples for frequencies in the range 1 Hz $\leqslant \nu \leqslant$ 1 kHz ($\mu_0 H_{ac} = 0.2$ mT). For $y = 0.1$, the dc-zfc susceptibility is additionally shown as a dashed line.

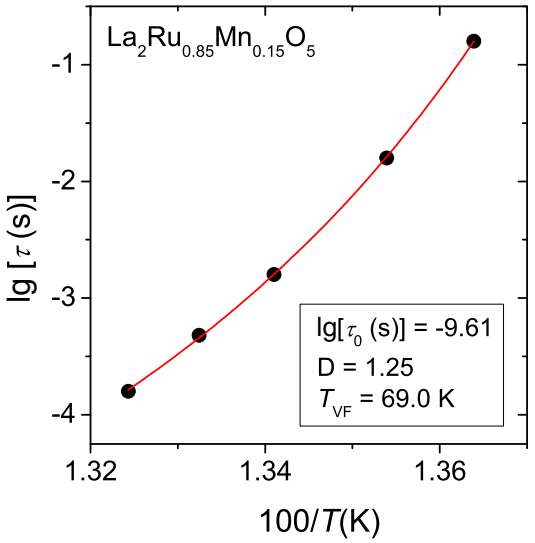

FIG. 6. (Color online) Logarithm of the inverse attempt frequency $\tau = 1/(2\pi\nu)$ as function of the inverse temperature for $La_2Ru_{0.85}Mn_{0.15}O_5$. The solid line indicates the fit using the Vogel-Fulcher-Tammann law. For details, see text.

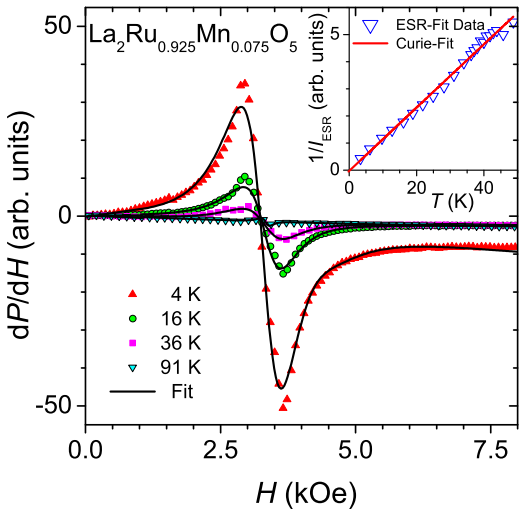

FIG. 7. (Color online) ESR spectra of $La_2Ru_{0.925}Mn_{0.075}O_5$ with Lorentz fits (solid lines) at selected temperatures. The inset shows the inverse ESR intensity ($1/I_{ESR}$) versus temperature. The solid line indicates the Curie law $1/I_{ESR} \propto T$.

freezing dynamics [39]. In this case, static freezing is predicted at a characteristic nonzero temperature.

To model the freezing in glassy systems and to quantify the characteristic temperature or frequency, one usually plots the peak maxima on a logarithmic scale as a function of the inverse temperature. In this representation, a simple thermally activated behavior results in a straight line (Arrhenius behavior). In Fig. 6, the logarithm of the characteristic relaxation time $\tau = 1/(2\pi\nu)$ (as determined by the peak maxima shown in Fig. 5) is given as a function of the inverse temperature. Obviously, the results do not correspond to a simple thermally activated Arrhenius behavior but have to be modeled using the Vogel-Fulcher-Tammann law $\tau = \tau_0 \exp(DT_{VF}/[T - T_{VF}])$ [39,40]. Here, τ_0 corresponds to an inverse characteristic microscopic frequency (attempt frequency), DT_{VF} characterizes a temperature-dependent energy barrier, and T_{VF} is the Vogel-Fulcher-Tammann temperature, at which the relaxation times diverge and a static freezing transition takes place. D reflects the curvature of the slope and is a standard parametrization in the physics of supercooled liquids. In this representation, Arrhenius behavior is recovered for $T_{VF} \to 0$ and $D \to \infty$. In addition, D characterizes the strength of the temperature dependence of the hindering barriers and consequently the growth of correlation length as approaching the spin-glass transition. The fit of the experimental values for $y = 0.15$ using the Vogel-Fulcher-Tamman law (solid line in Fig. 6) results in a convincing description with realistic parameters, which are indicated in the figure. The attempt frequency is of the order of GHz, a small value when compared to canonical spin glasses. The Vogel-Fulcher-Tamman temperature is rather high, the parameter D is almost unity, characteristic for a cooperative system close to static order. A small D is characteristic for deviations from Arrhenius behavior and indicates strong cooperativity, i.e., a drastic growth of cluster sizes when approaching the freezing transition.

3. Electron spin resonance

Further information on the magnetic properties at low temperatures is obtained from electron spin resonance (ESR) measurements. ESR detects the power P absorbed by the sample from the transverse magnetic microwave field as a function of the static magnetic field H. The signal-to-noise ratio of the spectra is improved by recording the derivative dP/dH using lock-in technique with field modulation. Figures 7 and 8 illustrate the generally different characteristics for low and high manganese concentration y, respectively. The border between the two regimes occurs gradually in the substitution range $0.1 \leqslant y \leqslant 0.15$. For $y < 0.1$, a pronounced resonance line of approximately Lorentz shape appears only below 80 K at a resonance field corresponding to $g \approx 2$ with a nearly constant linewidth $\Delta H \approx 500$ Oe. Data at selected

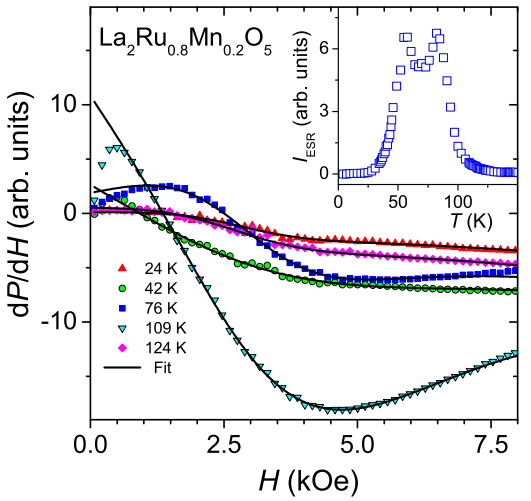

FIG. 8. (Color online) ESR spectra of $La_2Ru_{0.8}Mn_{0.2}O_5$ with Lorentz fits (solid lines) at selected temperatures. The inset shows the ESR intensity (I_{ESR}) as a function of temperature.

temperatures (symbols) and Lorentz-shape fits (solid lines) are shown in the main frame of Fig. 7 for $y = 0.075$, where the signal can be detected up to 50 K. The double-integrated signal intensity I_{ESR} follows a Curie law as depicted in the inset of Fig. 7 by its inverse representation $1/I_{ESR}$ as a function of temperature. This indicates that interactions between the magnetic centers, which give rise to the ESR signal, are negligible.

For $y > 0.15$, an extremely broad resonance line shows up at intermediate temperatures $30 \leqslant T \leqslant 120$ K (Fig. 8). As can be seen in the main frame, its approximation by a Lorentz shape has to be taken with caution as the linewidth reaches maximum values of about 8 kOe, which is much larger than the corresponding resonance field close to 3 kOe and below. Nevertheless, it is instructive to plot the ESR intensity I_{ESR} as a function of temperature. Like the ac susceptibility considered above, for different substitution levels, I_{ESR} exhibits a single maximum or a double-peak structure, as shown in the case of $y = 0.2$ in the inset of Fig. 8. At low temperatures, the intensity becomes suppressed indicating a frozen magnetic state where the spins can not follow the external excitation anymore.

Thus, the ESR results nicely show how the increasing manganese substitution first only locally disturbs and polarizes the dimerized Ru matrix, giving rise to paramagnetic centers. These practically do not interact because they are screened from each other by the neighboring dimers. For manganese concentrations above 10% the paramagnetic centers start to interact because of an increasing number of broken dimers, yielding a collective magnetic response in agreement with the ac-magnetic susceptibility. In principle, the shift of the maxima of the ESR intensity measured at 9.4 GHz with respect to those of the ac susceptibility taken up to kHz frequencies should allow us to extend the Vogel-Fulcher-Tammann law of Fig. 6. However, the uncertainty of the Lorentz fit due to the huge linewidth has so far prevented us from obtaining a conclusive result. Here, high-field ESR experiments in the submillimeter-wave regime would be necessary to extend the data.

B. Specific heat

To further characterize the phase transitions described in the sections above, the specific heat of selected $La_2Ru_{1-y}Mn_yO_5$ samples (y in steps of 0.05) was measured. From the susceptibility measurements it is known that for $y \geqslant 0.1$, both transitions, i.e., the spin dimerization and the spin-glass formation, are observed, while for $y = 0.25$ only the latter is found. The specific-heat data of the samples are depicted in Fig. 9 plotted as C_p/T versus temperature. To increase comparability, the curves were shifted in equidistant steps. The peak emerging from the Ru-spin dimerization is observed at 161 K for unsubstituted La_2RuO_5 and linearly shifts to lower temperatures with increasing y. For $y \geqslant 0.15$, the peak significantly broadens indicating increasing disorder in the low-temperature phase. This broadening and smearing out of the heat-capacity anomaly increases with higher Mn concentration until for $y = 0.25$ a clear peak can not be observed anymore and can only be recognized by a slight change of curvature at approximately 100 K.

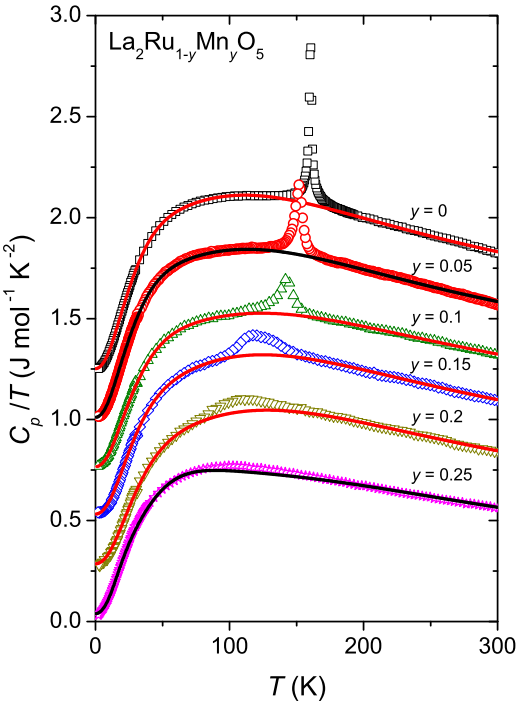

FIG. 9. (Color online) Specific heat in C_p/T representation of $La_2Ru_{1-y}Mn_yO_5$ for selected substitution levels. To increase comparability, the data were shifted in equidistant steps (0.25 J mol^{-1} K^{-2}). The corresponding Einstein-Debye fits of the phononic contribution are shown as solid lines.

A fit of the lattice contribution to C_p was carried out using an Einstein-Debye phonon model with one Debye and four Einstein terms [41]. Corresponding to the eight atoms per formula unit, eight terms were used according to the following weighting scheme: $1 \times \Theta_D + 1 \times \Theta_{E1} + 1 \times \Theta_{E2} + 1 \times \Theta_{E3} + 4 \times \Theta_{E4}$. The obtained fit values for the Debye temperature Θ_D and the Einstein temperatures Θ_{En} ($n = 1,2,3,4$) are listed in Table I. The values for La_2RuO_5 were already reported previously [26]. The fits are shown as solid lines in Fig. 9 and are in reasonable agreement with the experimental data. The Debye temperatures for all compounds are similar. Also, the four Einstein terms used for the fitting procedure are comparable. However, we were not able to derive a stable and reliable fit for the compound with manganese concentration $y = 0.25$. In this case, we had to use a constraint, namely, $\Theta_{E2} = \Theta_{E3}$. In addition, Θ_{E4} is rather large when compared to the results of the other concentrations. This probably results from the smeared out dimerization transition and a hidden spin-glass peak, which is expected in the same temperature range.

At very low temperatures, an increasing offset in C_p/T was observed, indicative of a linear-in-temperature contribution to the heat capacity, which in the fitting procedure was treated as an additional parameter c_0. In metals, this contribution corresponds to the Sommerfeld coefficient, which is directly linked to the electronic density of states at the Fermi energy [42]. In semiconductors, this contribution is expected to be zero at low temperatures. However, the specific heat in spin glasses varies approximately linearly with T for temperatures below T_f [38]. In addition, a broad peak

TABLE I. Results of the heat-capacity fit of $La_2Ru_{1-y}Mn_yO_5$. Θ_D and Θ_{En} ($n = 1,2,3,4$) are Debye and Einstein temperatures, respectively. c_0 characterizes a linear contribution to the specific heat. The magnetic entropy S_{mag} was calculated from the integrated residual after subtraction of the lattice contribution (for details see text).

Sample	c_0 $\left(\frac{mJ}{mol\,K^2}\right)$	Θ_D (K)	Θ_{E1} (K)	Θ_{E2} (K)	Θ_{E3} (K)	Θ_{E4} (K)	S_{mag} $\left(\frac{J}{mol\,K}\right)$
La_2RuO_5 (Ref. [26])	2.2	132	175	217	325	520	4.2(3)
$La_2Ru_{0.95}Mn_{0.05}O_5$	11	132	179	221	335	540	3.9(3)
$La_2Ru_{0.9}Mn_{0.1}O_5$	16.5	144	190	233	359	592	3.1(3)
$La_2Ru_{0.85}Mn_{0.15}O_5$	32	148	185	263	348	558	3.2(3)
$La_2Ru_{0.8}Mn_{0.2}O_5$	36	154	197	267	352	583	3.4(3)
$La_2Ru_{0.75}Mn_{0.25}O_5$	39	136	195	291	291	720	3.6(3)

is expected at roughly $1.2T_f$. The obtained values for c_0 are listed in Table I. The origin of the small but significant coefficient for unsubstituted La_2RuO_5 remains unclear. c_0 might be due to a finite density of electronic states at the Fermi level or due to frozen-out paramagnetic impurity spins in the dimerized phase of La_2RuO_5. With increasing manganese substitution level, c_0 increases to 39 mJ mol^{-1} K^{-2} for $y = 0.25$, signaling increasing importance of spin-glass contributions. On the other hand, there is no simple scaling of the linear contribution with the manganese concentration. Neither is any significant contribution of the spin-glass state to the heat capacity found at $\cong 1.2T_f$. However, for high substitution levels, this contribution is expected close to 100 K, where phonon contributions dominate the heat capacity and it might well be that these spin-glass contributions merge with the smeared-out peak of the dimerization transition.

Figure 10 shows the specific heat after subtraction of the lattice contribution in C_p/T versus T representation. For increasing Mn concentration y a shift of the peak, which is ascribed to the Ru dimerization, to lower temperatures is observed. Concomitantly, the peak height strongly decreases and the dimerization transition obviously becomes heavily smeared out. In the inset (a) of Fig. 10, the temperatures of the peak maxima are depicted as a function of the substitution level. The solid red line corresponds to $T = [166(1 - y)]$ K, which stems from a linear fit of the spin-dimerization transition temperatures up to $y = 0.175$ obtained from the magnetic

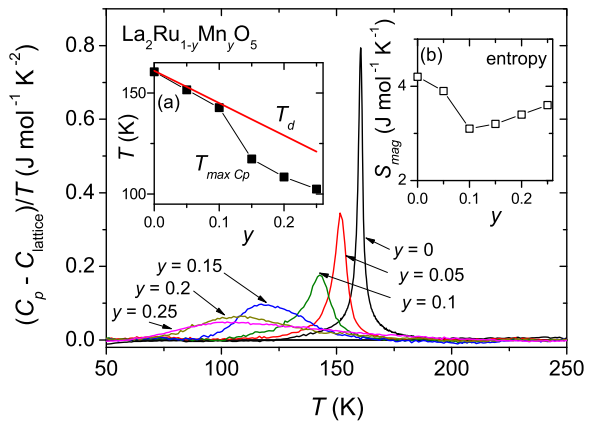

FIG. 10. (Color online) Residual specific heat $(C_p - C_{lattice})/T$ of $La_2Ru_{1-y}Mn_yO_5$ for the samples shown in Fig. 9. The insets show the temperatures of the peak maxima (a) and the entropy changes (b) as a function of the Mn concentration y.

susceptibility data as it was previously reported for Ti-substituted La_2RuO_5 [43]. For $y \geqslant 0.15$, the peak broadens significantly and the maximum shifts to values 20 K below the extrapolated dimerization temperatures. This shift might be caused by additional contributions of the spin-glass transition just below the dimerization temperature in the lt phase. From the peak areas, the magnetic entropy contribution S_{mag} was obtained via $S_{mag} = \int dT\ (C_p - C_{lattice})/T$ between 50 and 250 K. The obtained entropies are listed in the last column of Table I and are depicted in the inset Fig. 10(b). In the pure compound La_2RuO_5 the entropy is 4.2 J mol^{-1} K^{-1} which is approximately 50% of the entropy for spin $S = 1$ systems because of a residual degeneration of the dimerized ground state [26,44]. The decreasing entropy with increasing Mn concentration for $y \leqslant 0.1$ results from the dilution of Ru centers and further appearing Ru-Mn exchange interactions, which strongly compete with the Ru-Ru exchange. However, for $y \geqslant 0.15$ the entropy is increasing, probably due to an enhanced contribution of the spin glass to the transition peak, while the fraction of the dimerization transition is expected to decrease rapidly above $y = 0.1$ because structural changes strongly reduce the intradimer interaction strength.

C. Magnetic phase diagram

Using the experimental results of the previous sections, a magnetic phase diagram was derived and is shown in Fig. 11. The dimerization temperature T_d from the paramagnetic to the spin-singlet phase was determined from the inverse susceptibility curves as described in Ref. [45]. The obtained values (black circles) are depicted in Fig. 11 together with a linear fit (solid red line). The fit corresponds to a linear decrease of T_d down to 0 K for $y = 1$ following $T_d = [166(1 - y)]$ K. While up to $y = 0.15$ the T_d values can be well determined from the anomaly caused by the transition, for $0.15 < y \leqslant 0.2$ this becomes more difficult and leads to large error bars. Thus, these temperatures are only marked by open gray circles.

The freezing temperatures T_f of the spin-glass transition are indicated by solid blue triangles in Fig. 11. They were determined by the peak maxima of the real part of the ac susceptibility at measuring frequencies of 1 Hz. In case of two maxima, as observed for manganese contents $y \geqslant 0.15$ (Fig. 5), we indicated the second peak with the open blue triangles. We assume that the upper transition corresponds to the classical spin-glass freezing of individual spins, whereas the low-temperature maxima can be interpreted as blocking temperatures of partly ordered nanoclusters. As documented

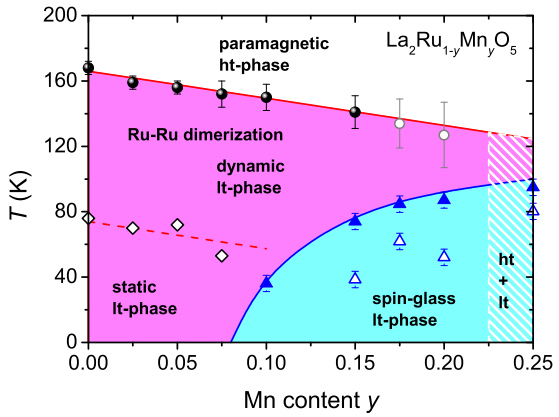

FIG. 11. (Color online) Phase diagram of $La_2Ru_{1-y}Mn_yO_5$. Solid black spheres and open gray circles mark the dimerization temperature T_d (dimerized lt phase is colored magenta) and the solid red line indicates a fit according to $T_d = [166(1 - y)]$ K. The open diamonds characterize the temperatures at which the singlet state with dynamic Ru-Ru dimers freeze-out and become static as found in ESR experiments. The blue solid and open triangles mark the peak maxima in the ac susceptibility measured at a frequency of 1 Hz and indicate the transition to the cyan colored spin-glass state. The white shaded area for $y \geqslant 0.225$ indicates the structural phase separation in ht and lt phases, which only appears at low temperatures.

in Fig. 1(a), the spin glass is characterized by a small ferromagnetic contribution. Hence, the broad distribution of exchange interactions is not centered around zero interaction strength but around a slight positive, i.e., ferromagnetic, value. For concentrations $y < 0.1$, no freezing transition was observable in the ac-susceptibility measurements.

The open diamonds were determined by the ESR measurements and mark the temperature above which no clear Lorentz-shaped ESR signal could be observed. The dashed red line marks this border in the phase diagram indicating the transition from a lt phase with dynamic Ru-Ru dimers to a static one, where only impurities and domain borders give rise to the ESR signal. In a first approximation, this line is parallel to the fit of the T_d data points. It still has to be clarified if this coincidence in temperature dependence really exists.

The phase diagram depicted in Fig. 11 illustrates the competition between Ru-Ru exchange (connected with a structural phase transition and a concomitant spin-singlet formation) and Ru-Mn as well as Mn-Mn exchanges establishing a low-temperature spin-glass state, which for $y > 0.1$ is a cooperative and percolating phenomenon. For manganese concentrations $0.1 \leqslant y \leqslant 0.2$, the spin-glass state coexists in the matrix of dimerized Ru-Ru singlet pairs. The spin-glass freezing of manganese and probably also of neighboring ruthenium spins occurs in the lt triclinic and dimerized phase. For $y = 0.25$, it was shown in Ref. [36] that only a fraction of the sample transforms to the lt structure, while about 55% remains in the ht modification (marked by the white shaded area in Fig. 11). At the spin-glass transition, the sample transforms into a spin glass coexisting with the triclinic lt phase, which is hard to interpret from the data of the used experimental methods. The interplay of both phases is not clear to our current knowledge, i.e., we assume that the monoclinic fraction remains paramagnetic without influencing the triclinic lt phase. In addition, it is not clear yet if the triclinic phase for $y = 0.25$ (clearly identified by temperature-dependent x-ray and neutron diffraction in Ref. [36]) is driven by the singlet formation: In the dc susceptibility [i.e., Fig. 1(b)] as well as from the heat capacity, we have no unambiguous experimental evidence for a dimerization. However, since the susceptibility is dominated by the paramagnetic contributions and the spontaneous magnetization below 120 K, a small transition step characterizing the dimerization is simply undetectable. Thus, it is very probable that the magnetic properties are determined by the fraction of the sample which transforms into the triclinic lt modification. On the other hand, at low Mn-substitution levels $y < 0.1$ single ruthenium or manganese spins and probably also Ru-Mn pairs with $S = \frac{1}{2}$ relax and freeze in the dimerized matrix and a cooperative spin-glass state can not establish.

The temperature-dependent appearance of several transitions for one substitution level seems to be a typical feature caused by Ru/Mn mixing. This behavior was also reported for other perovskitelike and layered compounds with mixed Ru/Mn occupation on the Ru or Mn site [1,15,19,46]. With respect to the impurity-induced long-range order in spin-dimer systems, the phase diagram of $La_2Ru_{1-y}Mn_yO_5$ reminds of the one of doped $CuGeO_3$ [34,47]. Pure $CuGeO_3$ is a one-dimensional spin-Peierls system with spin chains of antiferromagnetically coupled Cu^{2+} ($S = \frac{1}{2}$) spin moments undergoing dimerization at $T_{SP} = 14$ K to a singlet ground state [27]. Upon doping, a second phase transition into antiferromagnetic order is observed at lower temperatures T_N. This ordering temperature increases linearly with increasing doping level, while T_{SP} decreases linearly. At a certain dopant concentration, the spin-Peierls transition is suppressed and only the antiferromagnetic phase is observed. This is similar to $La_2Ru_{1-y}Mn_yO_5$, in which the dimerization transition was described as a two-dimensional spin-Peierls-like transition leading to a singlet ground state. Also, for $La_2Ru_{1-y}Mn_yO_5$ the dimerization temperature decreases linearly with increasing manganese concentration and a second order emerges at lower temperatures. The antiferromagnetic phase in doped $CuGeO_3$ is divided in a short-range magnetically ordered phase on the dimerized background up to the substitution level at which the spin-Peierls transition breaks down and a long-range-ordered antiferromagnet above this value [34]. The doping leads to evolution of antiferromagnetic polarized $S = \frac{1}{2}$ chain fragments with a typical correlation length. These clusters show a certain dynamic behavior within the spin-Peierls dimerized matrix depending on temperature and impurity concentration. When the correlation length is in the range of the average distance between two substituted ions, the long-range order sets in and the spin-Peierls transition becomes suppressed [48,49]. This is a behavior which also can be used to describe the different phases in $La_2Ru_{1-y}Mn_yO_5$. For low manganese concentrations $y < 0.1$, the dynamic behavior of the dimers freezes out below 80 K and results in a static-dimerized phase, in which only the undimerized spins (not only due to the dopants, but also due to domain walls such as, e.g., reported for pure $CuGeO_3$ in Ref. [48]) can be detected by ESR characterized by an intensity following the Curie law. For $y \geqslant 0.1$, the spin-glass phase caused by the substituent

Mn is found on the spin-dimerized Ru-Ru matrix similar to the antiferromagnetic phase in doped $CuGeO_3$ reported in Ref. [49]. This electronic phase separation is observable in $La_2Ru_{1-y}Mn_yO_5$ until a certain manganese concentration is reached at which even structural phase separation occurs ($y = 0.25$).

IV. SUMMARY AND CONCLUSION

In this work, we present detailed investigations of magnetic properties and specific heat of $La_2Ru_{1-y}Mn_yO_5$. dc- and ac-magnetic susceptibility and ESR experiments, as well as heat-capacity measurements, were performed between 2 K and room temperature for the complete stable substitution range $0 \leqslant y \leqslant 0.25$. We propose a phase diagram, documenting the competition between spin-glass freezing and dimerization.

In the ht paramagnetic phase, the Curie-Weiss behavior is characterized by Ru^{4+} ($S = 1$) and Mn^{4+} ($S = \frac{3}{2}$) local moments and the negative Weiss temperatures indicate dominating antiferromagnetic exchange. Up to manganese concentrations of $y = 0.15$, we find clear experimental evidence for a homogeneous transition into a dimerized state with triclinic symmetry and Ru-Ru spin singlets. For $y < 0.1$, the emergence of ESR signals below 80 K caused by isolated magnetic centers suggest the freezing of magnetic fluctuations in this temperature regime but no second phase transition. In the temperature dependence of the heat capacity, we find evidence for the dimerization transition, for which the peak broadens considerably upon increasing Mn content. For $0.1 \leqslant y < 0.25$, field-cooled and zero-field-cooled measuring cycles as well as ac-susceptibility experiments identify a spin-glass transition at lower temperatures. The spin-glass state is a cooperative phenomenon, being established throughout the triclinic phase coexisting with the dimerized matrix. Furthermore, the spin glass is characterized by a considerable linear temperature dependence of the specific heat as usually found in spin-glass systems. Also, the transition peak broadens and shifts to lower temperature. For $y = 0.25$ spin-glass and dimerization transition compete and establish a phase separation into a (dimerized) lt-triclinic phase and a spin-glass state. The transition peak in the specific heat becomes extremely broad, in accordance with the vanishing steplike decrease of the magnetic dc susceptibility.

The similarities of $La_2Ru_{1-y}Mn_yO_5$ and doped $CuGeO_3$ reveal that the appearance of a second magnetic phase in a frozen-out singlet matrix is probably a general behavior for doped compounds providing a spin-Peierls transition. Thereby, the second phase is induced by the substituents and causes an electronic phase separation. In case of $La_2Ru_{0.75}Mn_{0.25}O_5$, this even leads to a structural separation.

ACKNOWLEDGMENTS

The authors gratefully acknowledge D. Vieweg for performing the SQUID measurements. This work was supported by the Bavarian graduate school (Resource strategy concepts for sustainable energy systems) of the Institute of Materials Resource Management (MRM) of the University of Augsburg and partly by the DFG within the collaborative research unit TRR 80 (Augsburg, Munich, Stuttgart).

[1] X.-Y. Zhang, Y. Chen, Z.-Y. Li, C. Vittoria, and V. G. Harris, J. Phys.: Condens. Matter **19**, 266211 (2007).
[2] G. Cao, S. Chikara, X. N. Lin, E. Elhami, V. Durairaj, and P. Schlottmann, Phys. Rev. B **71**, 035104 (2005).
[3] T. Ohnishi, M. Naito, S. Mizusaki, Y. Nagata, and Y. Noro, J. Electron. Mater. **40**, 915 (2010).
[4] S. S. Manoharan, H. L. Ju, and K. M. Krishnan, J. Appl. Phys. **83**, 7183 (1998).
[5] A. N. Vasil'ev and O. S. Volkova, Low Temp. Phys. **33**, 895 (2007).
[6] C. de la Calle, J. Sánchez-Benítez, F. Barbanson, N. Nemes, M. T. Fernández-Díaz, and J. A. Alonso, J. Appl. Phys. **109**, 123914 (2011).
[7] W. Kobayashi, I. Terasaki, J. Takeya, I. Tsukuda, and Y. Ando, J. Phys. Soc. Jpn. **73**, 2373 (2004).
[8] A. Krimmel, A. Günther, W. Kraetschmer, H. Dekinger, N. Büttgen, A. Loidl, S. G. Ebbinghaus, E.-W. Scheidt, and W. Scherer, Phys. Rev. B **78**, 165126 (2008).
[9] A. Krimmel, A. Günther, W. Kraetschmer, H. Dekinger, N. Büttgen, V. Eyert, A. Loidl, D. V. Sheptyakov, E.-W. Scheidt, and W. Scherer, Phys. Rev. B **80**, 121101(R) (2009).
[10] A. P. Ramirez, G. Lawes, D. Li, and M. A. Subramanian, Solid State Commun. **131**, 251 (2004).
[11] N. Buettgen, H.-A. Krug von Nidda, W. Kraetschmer, A. Günther, S. Widmann, S. Riegg, A. Krimmel, and A. Loidl, J. Low Temp. Phys. **161**, 148 (2010).
[12] R. Weht and W. E. Pickett, Phys. Rev. B **65**, 014415 (2001).
[13] A. Urushibara, Y. Moritomo, T. Arima, A. Asamitsu, G. Kido, and Y. Tokura, Phys. Rev. B **51**, 14103 (1995).
[14] Y. Moritomo, A. Asamitsu, H. Kuwahara, and Y. Tokura, Nature (London) **380**, 141 (1996).
[15] D. J. Gallon, P. D. Battle, S. J. Blundell, J. C. Burley, A. I. Coldea, E. J. Cussen, M. J. Rosseinsky, and C. Steer, Chem. Mater. **14**, 3976 (2002).
[16] J. E. Ortmann, J. Y. Liu, J. Hu, M. Zhu, J. Peng, M. Matsuda, X. Ke, and Z. Q. Mao, Sci. Rep. **3**, 2950 (2013).
[17] B. Hu, G. T. McCandless, V. O. Garlea, S. Stadler, Y. Xiong, J. Y. Chan, E. W. Plummer, and R. Jin, Phys. Rev. B **84**, 174411 (2011).
[18] F. Weigand, S. Gold, A. Schmid, J. Geissler, E. Goering, K. Dörr, G. Krabbes, and K. Ruck, Appl. Phys. Lett. **81**, 2035 (2002).
[19] B. Schüpp, K. Dörr, K. Ruck, K. Nenkov, K.-H. Müller, and G. Krabbes, Solid State Sci. **7**, 17 (2005).
[20] P. Khalifah, R. Osborn, Q. Huang, H. W. Zandbergen, R. Jin, Y. Liu, D. Mandrus, and R. J. Cava, Science **297**, 2237 (2002).
[21] P. Boullay, D. Mercurio, A. Bencan, A. Meden, G. Drazic, and M. Kosec, J. Solid State Chem. **170**, 294 (2003).
[22] S. K. Malik, D. C. Kundaliya, and R. D. Kale, Solid State Commun. **135**, 166 (2005).
[23] Hua Wu, Z. Hu, T. Burnus, J. D. Denlinger, P. G. Khalifah, D. G. Mandrus, L.-Y. Jang, H. H. Hsieh, A. Tanaka, K. S. Liang, J. W. Allen, R. J. Cava, D. I. Khomskii, and L. H. Tjeng, Phys. Rev. Lett. **96**, 256402 (2006).

[24] V. Eyert, S. G. Ebbinghaus, and T. Kopp, Phys. Rev. Lett. **96**, 256401 (2006).
[25] V. Eyert and S. G. Ebbinghaus, Prog. Solid State Chem. **35**, 433 (2007).
[26] S. Riegg, A. Günther, H.-A. Krug von Nidda, A. Loidl, M. V. Eremin, A. Reller, and S. G. Ebbinghaus, Phys. Rev. B **86**, 115125 (2012).
[27] M. Hase, I. Terasaki, and K. Uchinokura, Phys. Rev. Lett. **70**, 3651 (1993).
[28] R. J. Beynon and J. A. Wilson, J. Phys.: Condens. Matter **5**, 1983 (1993).
[29] A. Seidel, C. A. Marianetti, F. C. Chou, G. Ceder, and P. A. Lee, Phys. Rev. B **67**, 020405(R) (2003).
[30] R. Rückamp, J. Baier, M. Kriener, M. W. Haverkort, T. Lorenz, G. S. Uhrig, L. Jongen, A. Möller, G. Meyer, and M. Grüninger, Phys. Rev. Lett. **95**, 097203 (2005).
[31] M. Shaz, S. van Smaalen, L. Palatinus, M. Hoinkis, M. Klemm, S. Horn, and R. Claessen, Phys. Rev. B **71**, 100405(R) (2005).
[32] J. Hemberger, M. Hoinkis, M. Klemm, M. Sing, R. Claessen, S. Horn, and A. Loidl, Phys. Rev. B **72**, 012420 (2005).
[33] Y. Uchiyama, Y. Sasago, I. Tsukada, K. Uchinokura, A. Zheludev, T. Hayashi, N. Miura, and P. Böni, Phys. Rev. Lett. **83**, 632 (1999).
[34] K. Uchinokura, J. Phys.: Condens. Matter **14**, R195 (2002).
[35] A. I. Smirnov, V. N. Glazkov, H.-A. Krug von Nidda, A. Loidl, L. N. Demianets, and A. Ya. Shapiro, Phys. Rev. B **65**, 174422 (2002).
[36] S. Riegg, A. Loidl, F. J. Garcia Garcia, A. Reller, S. G. Ebbinghaus, Phys. Rev. B **90**, 024406 (2014).
[37] J. A. Mydosh, *Spin Glasses: An Experimental Introduction* (Taylor & Francis, London, 1993).
[38] K. Binder and A. P. Young, Rev. Mod. Phys. **58**, 801 (1986).
[39] J. L. Tholence, Solid State Commun. **35**, 113 (1980).
[40] C. A. Angell, J. Non-Cryst. Solids **102**, 205 (1988).
[41] R. P. Singh and C. V. Tomy, J. Phys.: Condens. Matter **20**, 235209 (2008).
[42] A. Tari, *The Specific Heat of Matter at Low Temperatures* (Imperial College Press, London, 2003).
[43] S. Riegg, S. Widmann, A. Günther, H.-A. Krug von Nidda, A. Reller, A. Loidl, and S. G. Ebbinghaus, J. Phys.: Condens. Matter **25**, 126002 (2013).
[44] S. Riegg, A. Günther, H.-A. Krug von Nidda, M. V. Eremin, A. Reller, A. Loidl, and S. G. Ebbinghaus, Eur. Phys. J. B **85**, 413 (2012).
[45] S. Riegg, U. Sazama, M. Fröba, A. Reller, and S. G. Ebbinghaus, Phys. Rev. B **84**, 014403 (2011).
[46] X.-Y. Zhang, Y. Chen, and Z.-Y. Li, J. Appl. Phys. **103**, 07B303 (2008).
[47] B. Grenier, J.-P. Renard, P. Veillet, L.-P. Regnault, J. E. Lorenzo, C. Paulsen, G. Dhalenne, and A. Revcolevschi, Phys. B (Amsterdam) **259–261**, 954 (1999).
[48] A. I. Smirnov, V. N. Glazkov, L. I. Leonyuk, A. G. Vetkin, and R. M. Eremina, J. Exp. Theor. Phys. **87**, 1019 (1998).
[49] A. I. Smirnov and V. N. Glazkov, J. Exp. Theor. Phys. **105**, 861 (2007).